Journal of Analytical and Applied Pyrolysis 196 (2026) 107756

Contents lists available at ScienceDirect

Journal of Analytical and Applied Pyrolysis

journal homepage: www.elsevier.com/locate/jaap

Tracing the source and transformations of organic matter in a Mars analogue lava tube using Py-CSIA

Nicasio T. Jiménez-Morillo [a], Layla M. San-Emeterio [b], José M. De la Rosa [a], José A. González-Pérez [a], Francesco Sauro [c], Ana Z. Miller [a,*]

[a] Instituto de Recursos Naturales y Agrobiología de Sevilla, Consejo Superior de Investigaciones Científicas (IRNAS-CSIC), Av. Reina Mercedes 10, Sevilla 41012, Spain
[b] Department of Soil and Environment, Swedish University of Agricultural Sciences (SLU), Lenmart Hjelms Väg 9, P. O. Box 7014, Uppsala 75007, Sweden
[c] Department of Geosciences, University of Padova, Italy

ARTICLE INFO

Keywords:
Volcanic caves
Speleothems
Mass spectrometry
Stable isotope
Analytical pyrolysis
Astrobiology

ABSTRACT

Volcanic speleothems are promising archives of organic matter (OM) in planetary analogue environments, offering valuable insights into past or extant microbial life and environmental conditions. In this study, we applied elemental analysis–isotope ratio mass spectrometry (EA/IRMS), analytical pyrolysis (Py-GC/MS), and pyrolysis-compound-specific isotope analysis (Py-CSIA) to characterize the molecular and isotope composition of four samples collected from the Corona Lava Tube system in Lanzarote (Canary Islands, Spain). This site, explored during the ESA PANGAEA-X astronaut training campaign, serves as a natural laboratory for Mars subsurface analogues. We investigated two distinct cave samples (a black, organic-rich microbial mat and a white, mineral-dominated deposit), along with overlying topsoil and *Euphorbia balsamifera* vegetation, to trace the origin, transformation, and preservation of OM in this extreme subsurface environment. Stable isotope data and compound-specific signatures revealed marked differences in carbon and hydrogen isotope compositions between surface- and cave-derived organics, indicating divergent biogeochemical pathways and microbial activity. Notably, ^{1} ^{3}C-enrichment in sterols and lignin-derived compounds within the cave matrix pointed to intense microbial processing, while δ^{2}H data reflected the incorporation of past meteoric water and diagenetic alteration. Our findings demonstrate the power of Py-CSIA for resolving biosignatures at the molecular level and underscore the diagnostic potential of isotope tools in volcanic subsurface systems. This approach provides a critical framework for future astrobiological exploration and life-detection strategies in Martian lava tubes, where subtle organic traces may offer the clearest evidence of habitability or life beyond Earth.

1. Introduction

The Corona Lava Tube System, located on the volcanic island of Lanzarote (Canary Islands, Spain), is one of the largest and most geologically complex lava tubes on Earth [1]. Formed during Late Pleistocene volcanic activity, it features subterranean passages lined with secondary mineral deposits, or speleothems, that preserve records of geological and biological processes. The arid climate, minimal soil cover, and basaltic terrain of Lanzarote closely resemble conditions expected in lava tubes on the Moon and Mars [2,3], making the Corona system an exceptional planetary analogue for studying habitability and biosignature preservation, as well as the implementation of different molecular and isotope techniques.

Despite the potential of isotope-based approaches for astrobiology, their application in lava tube environments remains limited. Techniques such as those implemented in the Mars Organic Molecule Analyzer (MOMA), onboard the Rosalind Franklin rover in the forthcoming ExoMars mission, currently focus on molecular composition [4], but incorporating isotope analysis could reveal the origin of organic molecules and past environmental changes, enhancing biosignature detection [5].

Speleothems in volcanic caves can preserve organic matter from surface inputs and *in situ* microbial activity [6,7], but resolving its biogenicity requires high-resolution approaches, such as traditional bulk stable isotope analysis (EA/IRMS), analytical pyrolysis (Py-GC/MS) and pyrolysis-compound-specific isotope analysis (Py-CSIA). In light of this, stable isotope analysis of light bioelements (e.g., C, N, O and H) is a powerful tool for tracing the origin and transformation of organic matter

* Corresponding author.
E-mail address: anamiller@irnas.csic.es (A.Z. Miller).

https://doi.org/10.1016/j.jaap.2026.107756
Received 2 June 2025; Received in revised form 6 February 2026; Accepted 17 March 2026
Available online 18 March 2026

(OM) through biosynthetic fractionation patterns [8]. Nevertheless, while bulk isotope analysis provides general information on carbon and hydrogen sources, it averages signals from all organic components, obscuring molecular-level variation critical for linking isotope patterns to microbial and environmental processes [6,7,9,10]. To overcome these limitations, pyrolysis-compound-specific isotope analysis (Py-CSIA) offers a more targeted approach, allowing discrimination between biotic and abiotic sources and insights into environmental conditions [11–13]. Concerning the discrimination between biotic and abiotic sources for hydrogen (δ^2H) Py-CSIA, this method can help discriminate biotic from abiotic sources because δ^2H values are largely controlled by how hydrogen is incorporated during formation and the associated isotope effects. In biotic molecules (e.g., lipids), hydrogen is primarily derived from environmental water and intracellular reducing power (notably NADPH), and enzymatic reactions impose pathway-specific kinetic isotope fractionations that generate internally consistent δ^2H patterns across compound suites [14–17]. In contrast, abiotic organic molecules produced by non-enzymatic reactions (e.g., Fischer–Tropsch-type synthesis) incorporate hydrogen under different kinetic/thermodynamic controls that depend on temperature and catalysts, often yielding δ^2H signatures and inter-compound relationships that do not match biosynthetic fingerprints [18]. Finally, post-formation hydrogen isotope exchange with water under hydrothermal conditions can overprint primary δ^2H values, which must be considered when interpreting abiotic/thermogenic systems [19]. These differences are crucial for reconstructing the provenance, transformation, and diagenetic history of OM and water, as well as for linking isotope variations to microbial processes and environmental conditions.

In this study, we present the first application of Py-CSIA for carbon and hydrogen isotope analysis of organic molecules preserved in speleothems from the Corona Lava Tube System. We aim to investigate whether the preserved organic matter includes diagnostic molecular biomarkers of microbial origin, thereby providing evidence of past or extant subsurface microbial life in this Mars-analogue setting. Furthermore, we explore whether the hydrogen isotope composition of these individual compounds reflects distinct environmental water sources and microbial metabolic pathways, offering new insight into biogeochemical cycling in volcanic caves. Finally, we hypothesise that the successful application of Py-CSIA in the Corona system can serve as a methodological framework for future life-detection strategies in Martian lava tubes, significantly advancing the capabilities of astrobiological exploration.

2. Material and methods

2.1. Site description and sampling

The samples analysed in this study were collected during the European Space Agency's PANGAEA-X (Planetary ANalogue Geological and Astrobiological Exercise) astronaut training campaign, conducted in the Corona Lava Tube system on Lanzarote (Canary Islands, Spain). This site is a well-established terrestrial analogue for Martian subsurface environments due to its basaltic geology, arid climate, and preserved speleothem formations [1,2]. The Corona Lava Tube system is a multi-kilometer volcanic cave network, formed by basaltic lava flows originating from the Corona volcano, with multiple chambers separated by skylight entrances (*jameos*) [2].

Field sampling followed a multidisciplinary protocol aimed at simulating planetary exploration conditions, including astronaut-led microbiological and mineralogical collection under contamination-aware procedures [20].

Four representative samples were selected to explore the diversity of organic matter inputs and transformations across surface and subsurface compartments from the *Jameo de la Puerta Falsa* (Fig. 1). These include: (i) a black, sticky microbial mat collected from a large basaltic boulder in the twilight zone of the Corona Lava Tube (sample ID: CLT1; Fig. 1A); (ii) white, cotton-like secondary mineral deposits from the dark zone approximately 200 m from the cave entrance (sample ID: CLT3; Fig. 1B);

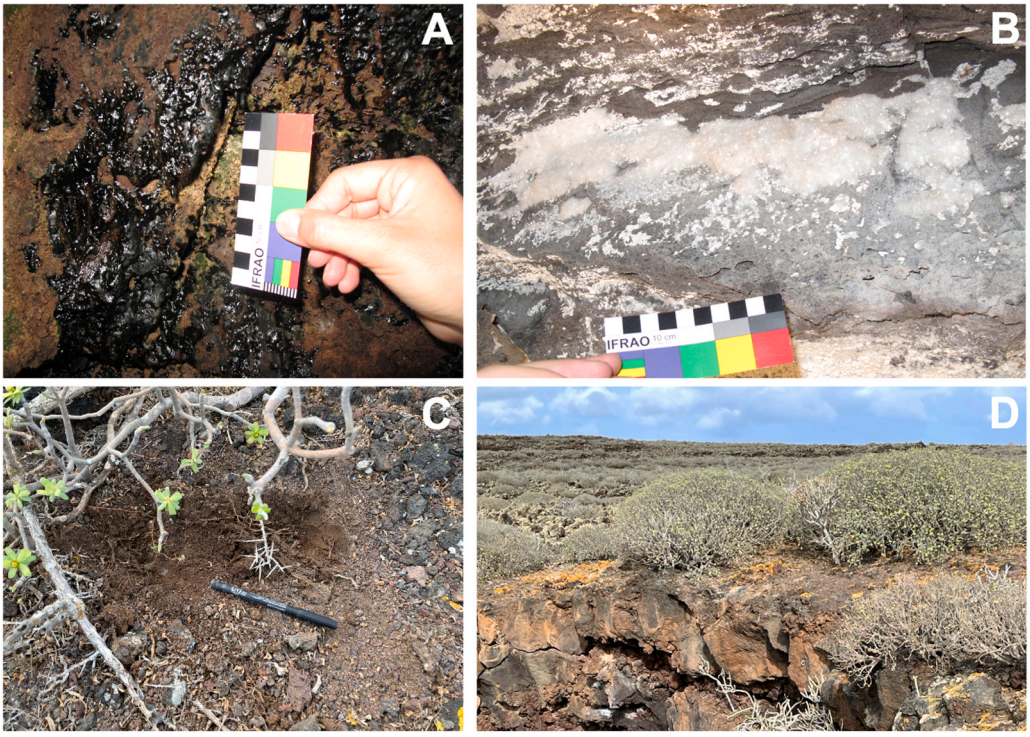

Fig. 1. Sampling locations and material types analysed in this study: A) Black, sticky jelly-like microbial mat (CLT1) collected from a large basaltic boulder in the twilight zone of the Corona Lava Tube; B) White cotton-like secondary mineral deposits (CLT3) located at the ceiling-wall interface approximately 200 m from the entrance in the dark zone; C) Topsoil (SCLT) collected directly above the lava tube entrance; D) Stem fragments of *Euphorbia balsamifera* (PCLT).

(iii) composite topsoil collected from directly above the lava tube (sample ID: SCLT; Fig. 1C), and stem fragments of *Euphorbia balsamifera*, the dominant vegetation on the surface (sample ID: PCLT; Fig. 1D), to trace the origin of OM in the cave samples.

All samples were collected in triplicate using sterile tools and stored in sterile containers for transport. Subsurface materials (CLT1 and CLT3) were taken using sterile disposable scalpels and transferred into 50 mL sterile tubes. Topsoil was gathered with sterile polypropylene scoops from the upper 0–10 cm across a 0.5 m diameter area and combined into a single homogenized composite (~100 g) in a sterile Whirl-Pak® bag. Vegetation material was clipped using ethanol-sterilized scissors and placed in sterile polypropylene containers.

2.2. Biogeochemical characterization

2.2.1. Elemental analysis / isotope ratio mass spectrometry (EA/IRMS)

The bulk carbon, nitrogen, and hydrogen isotope composition ($\delta^{13}C$, $\delta^{15}N$, and $\delta^{2}H$, respectively) was determined as described by [9,21] and San-Emeterio et al. [22]. In short, an elemental micro-analyzer (Flash 2000 HT, Thermo Scientific, Bremen, Germany) with reactors for combustion (C and N determinations) and for pyrolysis (H determination) was used, combined with a continuous flow isotope ratio mass spectrometer (IRMS, Delta V Advantage, Thermo Scientific, Bremen, Germany) via a ConFlo IV interface unit (Thermo Scientific, Bremen, Germany). Helium (He) was used as carrier gas at a flow rate of 80 mL min^{-1} for C and N, and 120 mL min^{-1} for H isotope analyses.

Prior to stable isotope analysis, soil (SCLT) and cave (CLT1 and CLT3) samples were decarbonated following the process described by Palma et al. (2024). Briefly, approximately 20 mg of soil and cave samples were ground to a fine powder, homogenised in a ball mill and treated with 1 *M* HCl for 24 h at room temperature. Acid rests were eliminated via repeated washes with distilled water until pH 5–6 was reached, then washed and dried (40 ºC, 48 h). Vegetation samples were oven-dried at 40 °C for 48 h, ground to a fine powder using a ball mill, and analysed directly without acid decarbonation.

The decarbonated cave (CLT1 and CLT3) and soil (SCLT) samples (0.5–5 mg) were weighed in metallic cups (IVA Analysentechnik GmbH & Co. KG, Meerbusch, Germany) made of tin for C and N, and of silver for H analyses. All samples were stored in a freezer at −20 °C until molecular and isotope analysis, to avoid the degradation of organic matter. Pure CO_2, N_2 and H_2 gas were inserted into the He carrier flow as pulses of the reference gas (250 mL min^{-1}). Cave and topsoil samples were decarbonated before IRMS analysis. Isotope analysis was carried out in triplicate ($n = 3$). Stable isotope results are expressed in the delta notation (δ) as parts per thousand deviations (‰) from corresponding international standards of Pee Dee Belemnite for carbon ($^{13}C/^{12}C$, PDB), Vienna-Air (V-Air) for nitrogen ($^{15}N/^{14}N$, V-Air), and Vienna Standard Mean Ocean Water (V-SMOW) for hydrogen ($^{2}H/^{1}H$, VSMOW), which are recognized by the International Atomic Energy Agency (IAEA). The standard deviation of bulk $\delta^{13}C$, $\delta^{15}N$ and $\delta^{2}H$ were ± 0.04‰, ± 0.2‰ and ± 1.0‰, respectively. The $\delta^{2}H$ stable isotope data of the samples were compared with the Global Network of Stable Isotopes in Precipitation (GNIP) from the IAEA.

2.2.2. Pyrolysis-gas chromatography/mass spectrometry

Analytical pyrolysis (Py-GC/MS) was performed using a 2020i double-shot pyrolyser (Frontier Labs, Fukushima, Japan) attached to a gas chromatography/mass spectrometry (GC/MS) system, as described by Miller et al. [5,23]. Briefly, approximately 10 mg of each sample (cave samples, topsoil and plant biomass) was introduced into crucible capsules and pre-heated for 1 min in a micro-furnace at 400 °C for pyrolysis. The compounds evolved were then directly injected into an Agilent 6890 N gas chromatograph (Agilent Technologies Wilmington, DE, USA), which was equipped with a HP-5ms-UI capillary column of 30 m × 250 µm × 0.25 µm film thickness (Agilent Technologies, Basel, Switzerland), and an Agilent 5973 mass selective detector (Agilent Technologies Wilmington, DE, USA). The chromatographic temperature ramp was held at 50 °C for 1 min and then increased to 100 °C at 30 °C min^{-1}, from 100 °C to 300 °C at 10 °C min^{-1}, and stabilised at 300 °C for 10 min. The mass spectra were acquired at 70 eV ionising energy, working at negative mode. Compound identification was attained by comparison with mass spectra library (NIST20 and Wiley7) using the Agilent MSD ChemStation Data Analysis software. According to numerous studies, the molecular products released by pyrolysis–gas chromatography/mass spectrometry (Py-GC/MS) can be traced to specific biogenic precursors: methoxyphenols indicate lignin; furans derive from polysaccharides; nitrogen-containing compounds (e.g., indoles) reflect proteins; and sterols, *n*-alkanes/alkenes, and fatty acids are characteristic of lipids [24-28]. This pattern arises because natural organic matter is a heterogeneous assemblage of compounds from diverse origins; upon thermal bond scission, the resulting fragments share core structures that map onto these compound classes. For example, pyrolysis of lignin yields methoxyphenol monomers that are widely accepted as lignin markers, just as indole-type N-containing products are commonly taken as indicators of protein degradation. In this work, we sorted the different organic compounds into 7 organic families, including aromatics, fatty acids, lignin, lipids, nitrogen compounds, sterols, and polysaccharides. The atomic ratios (H/C and O/C) of specific pyrochromatographic compounds were calculated from the empirical formulas inferred from the mass spectrometry information to generate contour density van Krevelen diagrams [29]. Chromatographic yields were normalized to the total area of identified compounds, and the relative abundances are represented as contour van Krevelen diagrams (Fig. 2), which are shown as density surfaces in the *x,y* plane defined by its atomic H/C (y-axis) and O/C (x-axis) ratios. A semi-quantification of the products released by analytical pyrolysis was done for each sample by converting the peak areas to a percentage of the total chromatographic area. Minor compounds with < 0.2% of the total chromatographic area were excluded.

2.2.3. Pyrolysis-compound-specific isotope analysis

The carbon ($\delta^{13}C$) and hydrogen isotope composition ($\delta^{2}H$) of individual compounds from the plant stems, topsoil and cave samples were determined by direct pyrolysis-compound-specific isotope analysis (Py-CSIA). This was performed using a double-shot pyrolyzer (Frontier Laboratory, model 3030D) linked to a Trace GC Ultra system (Thermo Scientific), which is connected to a GC-IsoLink II system (Thermo Scientific). The GC-Isolink II is equipped with two micro-reactors, one for pyrolysis (TC, Hydrogen determination), set at 1420 °C, and another for combustion (C, Carbon determination), set at 1020 °C. The Py-GC-Isolink system is coupled to a Delta V Advantage isotope ratio mass spectrometer (Thermo Scientific) via a ConFlo IV universal interface (Thermo Scientific). The samples were weighed (range to 0.5 and 5 mg) and placed into small pyrolysis capsules (Frontier Laboratory). The samples, in the capsules, were pyrolyzed into a pre-heated furnace at 400 °C, with an interface at 250 °C, for 1 min. The evolved gases were directly injected into the GC/IRMS for analysis.

Trace GC Ultra system was equipped with a low polar-fused silica (5% phenyl-methylpolysiloxane) capillary column Thermo DB5, of 30 m × 250 µm × 0.25 µm film thickness. The same chromatographic conditions used for Py-GC/MS were applied to Py-CSIA. This allows for the comparison and matching of the mass spectra obtained from both methods, which helps to infer the structural features of specific chromatographic compounds ([5,30]; San-Emeterio et al., 2023).

For $\delta^{13}C$ and $\delta^{2}H$ measurements, each chromatographic compound passing through the combustion and pyrolysis micro-reactor, respectively, are gasified including the analyte of interest CO_2 and H_2 gases, respectively. Pure CO_2 and H_2 gases are mixed into the He carrier flow, at ConFlo, as pulses of reference gas. In the case of hydrogen, before measuring the $^{2}H/^{1}H$ ratio, the $[H_3]^+$ factor is verified to be < 10 ppm/nA before every run. The variation of the $[H_3]^+$ factor during one run and between days is regularly checked to ensure a standard deviation

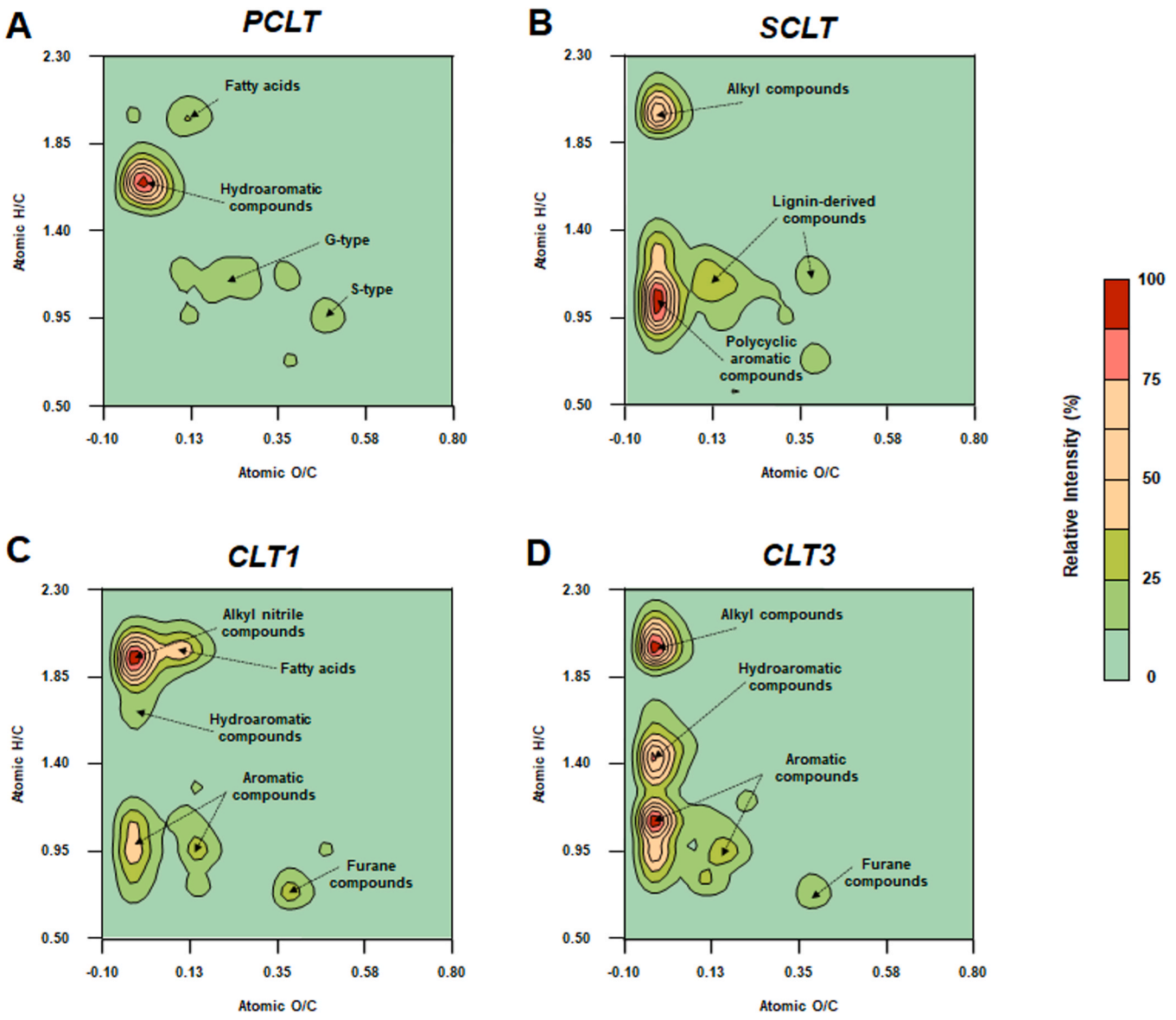

Fig. 2. Contour van Krevelen diagrams of: A) *Euphorbia balsamifera* plant stems (PCLT); B) Topsoil (SCLT); C) Black, sticky jelly-like mat (CLT1), and D) White secondary mineral deposits (CLT3). The diagrams show normalised relative abundances of pyrolysis-derived compounds represented as density surfaces in the *x*–*y* plane defined by their atomic O/C (x-axis) and H/C (y-axis) ratios.

lower than the unit for the whole measuring period [21]. Due to the limited sample quantity of CLT3, Py-CSIA analysis could not be performed on this sample.

The stable isotope abundances are reported in the delta (δ) notation (e.g. $\delta^{13}C$ and $\delta^{2}H$) in "parts per thousand" (‰). The carbon ($\delta^{13}C$) and hydrogen ($\delta^{2}H$) isotope values were calibrated against a saturated *n*-alkanes mixture, using the reference substance A7 (Biogeochemical Laboratories, Indiana University, U.S.A). The standard deviation of repeatability and reproducibility of $\delta^{13}C$ were ± 0.01 and 0.10‰, respectively, while for $\delta^{2}H$ were ± 0.08 and 0.23‰, respectively. Background subtractions, and isotope carbon and hydrogen compositions were calculated using the ISODAT 3.0 software (Thermo Scientific, Bremen, Germany). The $\delta^{13}C$ and $\delta^{2}H$ isotope values reported for each organic family (e.g., aromatics, lipids, polysaccharides) were calculated as the mean of the isotope values measured for the individual compounds assigned to that family (Table S3).

3. Results

3.1. Bulk stable isotope composition

The $\delta^{13}C$ values determined by EA/IRMS revealed differences between the cave samples (CLT1 and CLT3), topsoil (SCLT), and *E. balsamifera* stems (Table 1). The topsoil and plant exhibited similar

Table 1
Bulk isotope values ($\delta^{13}C$, $\delta^{15}N$, and $\delta^{2}H$) of decarbonized samples (mean ± STD in % and ‰, respectively).

Sample ID	$\delta^{13}C$ (‰, VPDB)	$\delta^{15}N$ (‰, V-Air)	$\delta^{2}H$ (‰, VSMOW)
PCLT (Plant stems)	-23.8 ± 0.1 b	15.1 ± 0.6 b	-62.4 ± 1.0 b
SCLT (Topsoil, 0–5 cm)	-24.1 ± 0.4 b	19.8 ± 1.0c	-46.4 ± 1.0c
CLT1 (Black organic coating)	-16.1 ± 0.3 c	11.2 ± 0.4 a	-23.5 ± 2.7 d
CLT3 (White mineral deposits)	-33.9 ± 0.2 a	21.9 ± 1.0 d	-75.9 ± 2.4 a

One-way ANOVA: The different letters indicate significant ($p < 0.05$) differences between samples according to the Tukey test.

$\delta^{13}C$ values. The $\delta^{13}C$ value of CLT3 (−33.9‰) is the most depleted among all the samples, while CLT1 showed the most enriched δ^{1} ^{3}C value (−16.1‰). Concerning $\delta^{15}N$, the topsoil (SCLT) exhibited higher values than PCLT (Table 1). The speleothem samples revealed contrasting $\delta^{15}N$ signatures: CLT1 showed a lower value (11.2‰), while CLT3 displayed the highest value among all samples (21.9‰). The $\delta^{2}H$ values also varied considerably between samples. The topsoil and plant stems showed $\delta^{2}H$ values of −46.4‰ and −62.4‰, respectively. CLT1 exhibited a significant ^{2}H-enrichment ($\delta^{2}H = -23.5$‰), whereas CLT3 exhibited a markedly depleted $\delta^{2}H$ value (−75.9‰).

Elemental analysis of carbon (C) and nitrogen (N) revealed distinct compositions among the samples: PCLT (plant stems) contained 42.6% C and 0.4% N; SCLT (topsoil) contained 3.2% C and 0.3% N; CLT1 (black organic coating) contained 13.1% C and 5.3% N; and CLT3 (white gypsum needles) contained 0.7% C and 0.2% N [31].

3.2. Molecular composition of organic matter by Py-GC/MS

Analytical pyrolysis (Py-GC/MS) revealed clear differences in the molecular composition of the organic matter (OM) among the cave samples (CLT1 and CLT3), topsoil (SCLT), and *Euphorbia balsamifera* stems (PCLT). The relative abundance and distribution of the main organic families are displayed in the contour van Krevelen diagrams in Fig. 2.

The molecular composition of *E. balsamifera* stems (PCLT) revealed a clear dominance of polysaccharides (furfurals and furanes), lignin-derived compounds (G- and S-types), fatty acids, *n*-alkanes, and a series of diterpenes, sterols, flavonoids, and other polyphenols (Fig. 2A, Table S1). Within the sterol family, we found compounds such as germanicol, stigmasta-3,5-dien-7-one, sitosterol, taraxasterol, and friedelan-3-one (Table S1).

The soil sample (SCLT) contained nitrogen-containing compounds (pyridine and methyl-pyridines), a series of long-chain *n*-alkanes, and aromatic compounds (e.g., 2,4-dimethylphenol, *p*-cresol, styrene), including polycyclic aromatic hydrocarbons (PAHs) such as 1,3-dimethylnaphthalene, 2,3,6-trimethylnaphthalene, 1,6-dimethyl-4-(1-isopropyl)naphthalene, and 9H-fluoren-9-one (Fig. 2B, Table S1). Furans and lignin derivatives, also identified in PCLT, were also detected in the soil sample

The cave samples CLT1 and CLT3 shared molecular fingerprinting: furans, nitrogen-containing compounds and *n*-alkanes, but differed in relative abundances (Fig. 2C,D, Table S1). CLT1 displayed a greater abundance of furans and fatty acids, whereas CLT3 contained more aromatic and hydroaromatic compounds, mainly derived from benzene. Several alkyl nitriles were also detected in CLT1.

3.3. Isotopic composition of organic compounds revealed by Py-CSIA

3.3.1. Carbon isotope ($\delta^{13}C$) composition

Fig. 3 displays the C isotope ($\delta^{13}C$) composition of the main specific organic compounds (Fig. 3A), the one-way ANOVA of $\delta^{13}C$ values (Fig. 3B), as well as the C isotope composition of the main 7 organic families (Fig. 3C) released by analytical pyrolysis from *E. balsamifera* stems (PCLT), topsoil (SCLT), and the cave samples (CLT1). Due to the limited amount of organic material in the CLT3 sample, the molecular compound signals fell below the detection threshold of the Py-CSIA technique, preventing C and H isotope composition for this sample.

In PLCT, most of the $\delta^{13}C$ values of specific compounds fall within the range of C_3 plants. The $\delta^{13}C$ values of in SCLT ranged between –23.9‰ and –19.8‰, broadly overlapping with those of PCLT (Fig. 3A,B). In

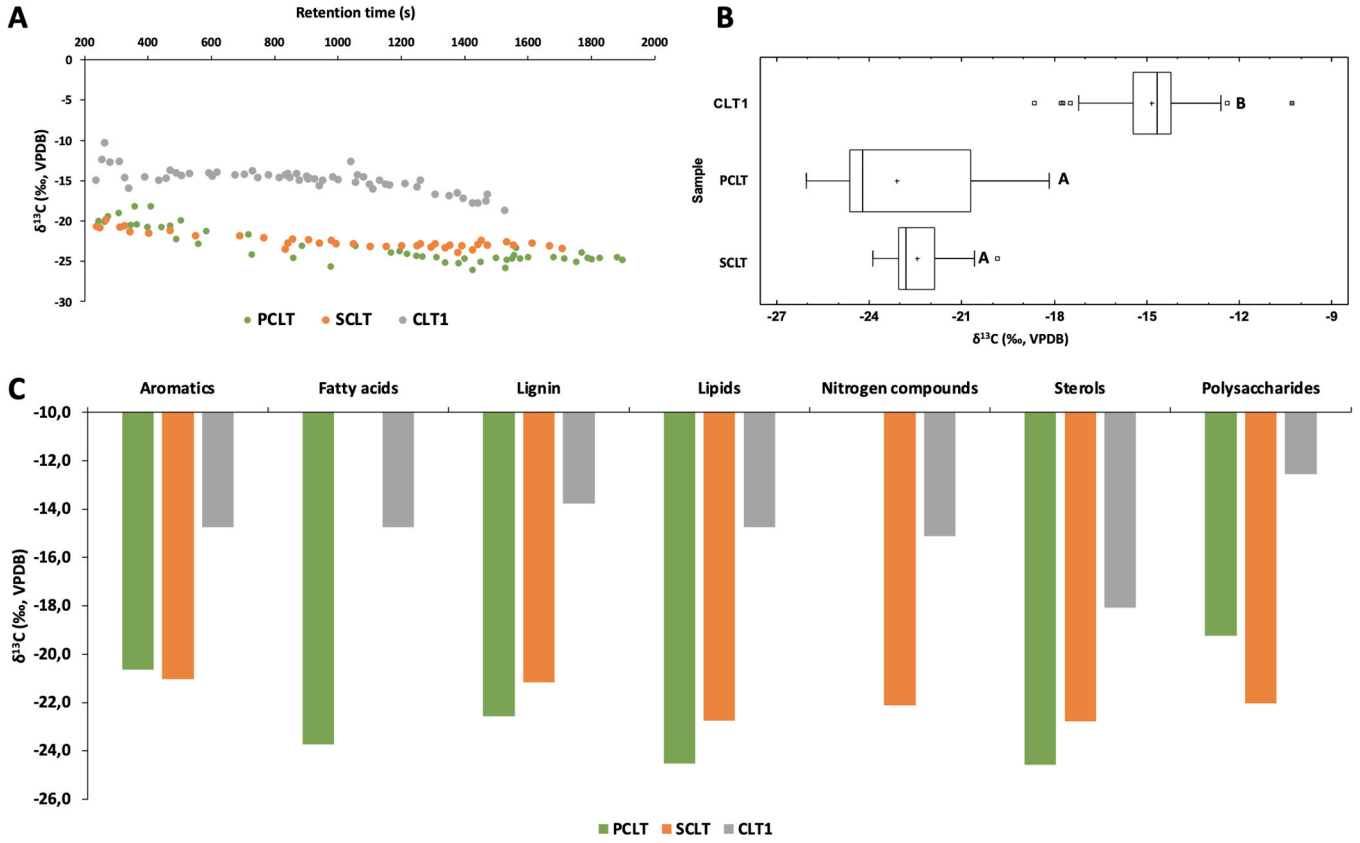

Fig. 3. Pyrolysis compound-specific isotope analysis of Carbon for *Euphorbia balsamifera* (PCLT), soil (SCLT), and the black jelly-like coating (CLT1) samples. A) Correlation plot between $\delta^{13}C$ (‰, VPDB) and chromatographic retention time (s); B) Boxplots of the carbon isotope values of chromatographic specific compounds, displaying the ranges, lower and upper quartiles (Q1, Q3), and the median (Q2). Box plots with different letters indicate significant differences (ANOVA; Means were compared using the Tukey test, $p = 0.05$); C) Carbon isotope ($\delta^{13}C$) composition of the main organic families.

contrast, the individual compounds from CLT1 showed markedly higher $\delta^{13}C$ values than those from the surface samples. Statistical comparison (one-way ANOVA) confirmed a significant ($p < 0.05$) ^{13}C-enrichment in CLT1 relative to PCLT and SCLT (Fig. 3B).

Compound-family averages revealed consistent patterns across samples (Fig. 3C). PCLT and SCLT showed relatively uniform $\delta^{13}C$ values across compound classes, whereas CLT1 exhibited pronounced ^{13}C -enrichment across all detected families. Within each sample, distinct isotope differences were also observed between compound classes. In PCLT, polysaccharides and aromatic compounds were more enriched than other families, while in SCLT lignin and aromatic-like structures were most enriched. In CLT1, sterols were significantly ^{13}C -enriched compared to polysaccharide-derived compounds (Table S3). For example, A-Neooleana-3(5),12-diene showed δ^{1} ^{3}C values of −25.1‰ (plant) and −23.0‰ (soil), compared to −16.7‰ in CLT1. Germanicol displayed values of −25.8‰ (plant) and −22.5‰ (soil), compared to −18.6‰ in CLT1.

3.3.2. *Hydrogen isotope (δ^2H) composition*

The hydrogen isotope signature (δ^2H) of specific compounds showed clear differences between surface and subsurface samples (Fig. 4). The correlation plot between δ^2H (‰, VSMOW) and chromatographic retention time (Fig. 4A) revealed that compounds in the cave sample (CLT1) were on average 30‰ more enriched than surface samples (PLCT and SCLT; Fig. 4B). By contrast, δ^2H values in the plant (PCLT) and topsoil (SCLT) samples were nearly identical (Fig. 4B). Both surface samples exhibited similar isotopic ranges, indicating consistent hydrogen isotope compositions within the surface organic matter pool.

Py-CSIA also provided δ^2H values for different compound families (Fig. 4C). In PCLT, carbohydrate-derived compounds (polysaccharides) displayed the highest isotope enrichment, while lipid compounds (*n*-alkanes/alkenes, fatty acids, and sterols) exhibited the lowest δ^2H values. Within lipids, sterols had the lightest hydrogen isotope composition compared to linear-chain lipids. Lignin-derived methoxyphenols showed enriched δ^2H values. In SCLT, δ^2H values were stable across all compound families, averaging around –60‰.

In CLT1, δ^2H values followed the same general trend as in PCLT but were markedly enriched. Lignin-like compounds (methoxyphenols) showed exceptionally high values (δ^2H_{lignin} CLT1 = –15.8‰), compared to –54.5‰ in PCLT and –61.1‰ in SCLT.

4. Discussion

The combined use of bulk isotope analyses (EA/IRMS), molecular fingerprinting by analytical pyrolysis (Py-GC/MS), and pyrolysis compound-specific isotope analysis (Py-CSIA) provided a multi-scale perspective on the sources and transformation of organic matter in the Corona Lava Tube. While bulk $\delta^{13}C$ and δ^2H values distinguished between surface-derived inputs and cave-associated materials, the molecular data from Py-GC/MS revealed the presence of diagnostic compounds (e.g., phenols, alkyl nitriles, lignin derivatives) that indicate both plant-derived precursors and microbial contributions. Py-CSIA further refined these interpretations by demonstrating carbon and hydrogen isotope enrichment patterns at the compound level, supporting the hypothesis of intense microbial reworking under variable redox conditions, as well as the hydrogen isotope fingerprint of past environments.

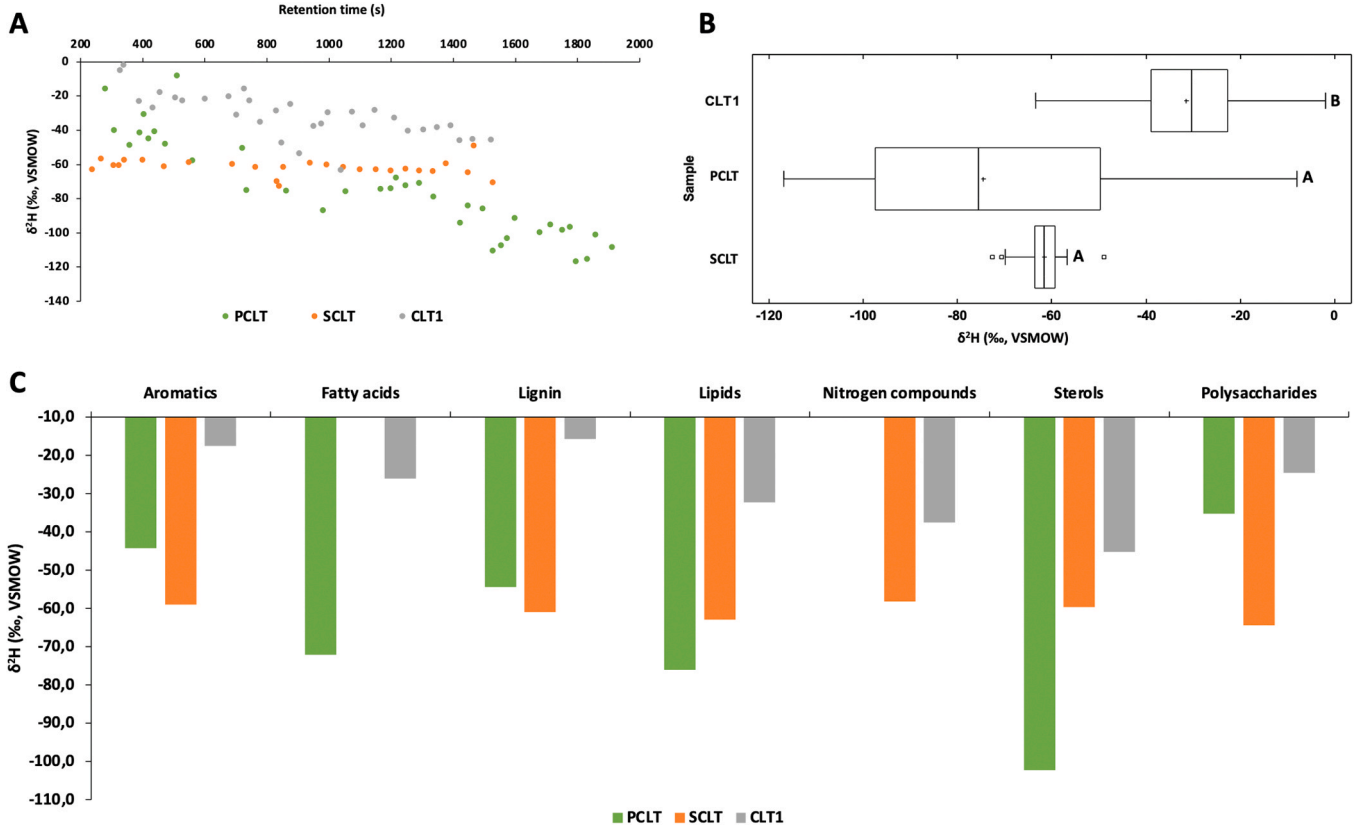

Fig. 4. Pyrolysis compound-specific isotope analysis of hydrogen for *Euphorbia balsamifera* (PCLT), soil (SCLT), and the black jelly-like coating (CLT1) samples. A) Correlation plot between δ^2H (‰, VSMOW) and chromatographic retention time (s); B) Boxplots of the hydrogen isotope values of chromatographic specific compounds, displaying the ranges, lower and upper quartiles (Q1, Q3), and the median (Q2). Box plots with different letters indicate significant differences (ANOVA; Means compared using the Tukey test, $p = 0.05$). C) Hydrogen isotope composition of the main organic families.

4.1. Bulk stable isotope signatures

The $\delta^{13}C$ values of PCLT and SCLT are consistent with organic matter inputs from C_3 vegetation [32], primarily from *Euphorbia balsamifera*, which typically exhibits $\delta^{13}C$ values of around −25‰ under arid conditions [33,34]. The relatively enriched $\delta^{13}C$ value of CLT1 (−16‰) likely reflects the combined influence of several processes, such as: i) the incorporation of latex-derived organic matter from *Euphorbia balsamifera*; ii) oxidative transformation and breakdown of latex-derived organic matter by microorganisms capable of degrading latex compounds and producing ^{1} ^{3}C-enriched byproducts [5,9,35], such as *Alcanivorax,* a genus previously identified in the Corona Lava Tube and known to metabolize lipid- and hydrocarbon-rich compounds derived from plant latex [31]; iii) the occurrence of organic compounds derived from C_4-plant leachates and preserved within the speleothem matrix [23]; and/or iv) the prevailing redox regime and microenvironmental conditions within the cave [36]. The darker coloration of CLT1, compared to the entirely white appearance of CLT3, is consistent with a higher content of microbially processed organic matter and supports these interpretations. In contrast, the strongly depleted $\delta^{13}C$ signature of CLT3 (−33.9‰) suggests a dominant contribution from specialized subsurface microbial communities, including taxa such as *Alicyclobacillus and Stenotrophomonas*, thriving under the atypical geochemical conditions of the Corona Lava Tube [31].

The bulk nitrogen isotope data further support the role of microbial transformations. Enriched $\delta^{15}N$ values in the topsoil relative to vegetation are consistent with isotope fractionation during microbial N cycling, including organic matter decomposition and nitrification [37,38]. The comparatively low $\delta^{15}N$ value in CLT1 (11.2‰) may reflect microbial alteration of plant-derived compounds [39]. In contrast, the highly enriched $\delta^{15}N$ in CLT3 (21.9‰) suggests intensive microbial cycling under oligotrophic conditions and possibly redox-variables conditions, consistent with extensive denitrification or volatilization processes within the deeper sections of the cave [40]. Miller et al. [31] reported the presence of *Stenotrophomonas* in the CLT3 sample, a taxon commonly associated with subsurface and cave environments and potentially involved in nitrate reduction, supporting the occurrence of active N redox transformations in this zone.

The hydrogen isotope results also point to contrasting sources and depositional processes. The enrichment in ^{2}H in the soil sample compared to plant tissues is consistent with evaporative enrichment of environmental water and associated biosynthetic effects [9,41]. The comparatively ^{2}H-enriched signal in CLT1 may reflect incorporation of isotopically evolved water and/or hydrogen from more processed organic matter, potentially linked to prolonged water-rock-organic interactions and microbial reworking within the cave environment [42,43]. In contrast, the depleted $\delta^{2}H$ values of CLT3 closely match the isotope signature of regional meteoric water reported for the area [44], which is consistent incorporation of rainfall-derived water into the speleothem matrix and potentially preserved in fluid inclusions. Multiple independent studies have demonstrated that speleothems can retain the hydrogen isotope signature of infiltrating (paleo)precipitation, providing a basis for interpreting speleothem $\delta^{2}H$ in terms of meteoric inputs [45–49]. These results highlight the potential of $\delta^{2}H$ measurements in volcanic speleothems to trace meteoric water contributions and to help contextualize the extent of subsequent microbial alteration of organic matter [50].

4.2. Molecular fingerprints by Py-GC/MS

The molecular profile of PCLT closely matched that of typical plant biomass, dominated by polysaccharides, lignin-derived methoxyphenols and a mixture of lipidic compounds, specifically *n*-alkanes/alkenes, fatty acids and sterols [25,51]. The sterol compounds (e.g., sitosterol, taraxasterol) are essential constituents of plant cell membranes, playing a critical role in regulating membrane fluidity, permeability, and structural stability, being essential for arid environments. Their primary function is to enhance cellular resilience against abiotic stressors, including drought and salinity [52,53].

In the topsoil sample (SCLT), the presence of long-chain *n*-alkanes, such as *n*-octacosane (C_{28}) and *n*-hentriacontane (C_{31}), confirms substantial inputs from epicuticular waxes of higher plants [6,24,54]. Of particular relevance are the condensed aromatic compounds (PAHs) concentrated in SCLT, as well as in CLT3 samples. PAHs can arise from multiple pathways: pyrogenic (incomplete combustion), petrogenic (fossil hydrocarbon inputs), direct biosynthesis by plants or microbes, or diagenetic/defunctionalization processes that transform lignin and other precursors into aromatic structures [55–57]. In the context of the Corona Lava Tube system, a pyrogenic origin for the observed PAHs is unlikely given the near-absence of recent burning indicators at the sampling sites; instead, low-molecular-weight PAHs in our samples are most plausibly derived from *in situ* transformation of plant-derived precursors (e.g., methoxyphenols to aromatics) and/or microbial biosynthesis (e.g., *Germmatimonadales*; [31]). This interpretation is consistent with: (i) the co-occurrence of lignin-derived markers and aromatics in CLT3, (ii) the depleted bulk and compound signals in some aromatic fractions, and (iii) the mineral matrix of CLT3, which can promote selective preservation of refractory aromatic material.

As easily distinguishable in the van Krevelen diagrams (Fig. 2C,D), the organic fraction of CLT1 sample may have a greater contribution from *E. balsamifera* (PCLT), highlighting the noticeable presence of long-chain fatty acids (epicuticular waxes), while CLT3 has a greater contribution from the andosol overlying the lava tube (SCLT). This finding is consistent with the data obtained from bulk stable isotope analysis (Table 1), which suggests the aboveground vegetation (*E. balsamifera*) as original source of organic fraction on the speleothem samples. In addition to phenolic and aromatic compounds, several alkyl nitriles were detected in CLT1. Moreover, the detection of alkyl nitriles in CLT1 is consistent with pyrolysis products of amino acids and other nitrogenous biomolecules [58,59], reinforcing the strong microbial imprint in this sample. Miller et al. [31] showed a number of reads analyzed in sample CLT1 (271347 reads) several orders of magnitude higher than in sample CLT3 (27626 reads). This aligns with its high nitrogen content and isotope evidence for microbial processing.

Given the strong interest in assessing whether the molecular signatures reported here are comparable to those obtained to date from Mars missions, Table S2 compiles a synopsis of the organic compounds detected on Mars by *in situ* rover analyses and provides a direct comparison with our molecular dataset (Table S1). To date, Martian organic detections include chlorobenzene and C_2–C_4 dichloroalkanes in Gale crater mudstones, together with thiophenes, benzene, toluene, and short-chain hydrocarbons; more recently, decane (C_{10}), undecane (C_{11}), and dodecane (C_{12}) have been reported and interpreted as pyrolysis products consistent with fatty-acid-like precursors [60,61]. Comparison with our results (Table S1) reveals overlap at the compound and/or class level, including benzene, toluene, and decane, as well as a broad suite of aromatic compounds (e.g., phenols/cresols, naphthalenes, fluorene derivatives) and lipid-related compounds/fatty acids (e.g., hexadecanoic, octadecanoic, and oleic acids). These molecular families are consistent with aromatic organics identified in Jezero crater [62]. In contrast, organochlorines (e.g., chlorobenzene/dichloroalkanes) and thiophenes were not detected in our samples, which is consistent with the view that some chlorinated species observed on Mars may be generated or enhanced during pyrolysis in the presence of oxychlorine phases (e.g., perchlorates) [60].

4.3. Isotope composition of specific molecules

The possibility of thermally induced isotope fractionation during analytical pyrolysis is considered unlikely under standard Py-CSIA conditions. Available evidence indicates that δ^{1} ^{3}C and $\delta^{2}H$ values of pyrolysis-derived compounds are not measurably altered by the

pyrolysis step, even when applied to different matrices and across typical operating temperatures [5,11,30,63]. This is generally attributed to the very short residence time of evolving products in the heated zone (≈1 min) and rapid transfer to the GC, which limits secondary reactions that could otherwise promote fractionation. Accordingly, our conditions (400 °C, 1 min) fall at the low end of the usual analytical pyrolysis range (ca. 300–600 °C) and are therefore not expected to modify the isotope composition of the compounds reported here.

4.3.1. Carbon isotope composition

The similarity of $\delta^{13}C$ values in PCLT and SCLT confirms that organic matter preserved in the soil sample is strongly derived from *E. balsamifera* [64], consistent with the bulk and Py-GC/MS data. The pronounced ^{13}C-enrichment of CLT1 compounds relative to surface samples (PCLT and SCLT) suggests intense microbial processing of organic matter, in line with previous reports that microbial metabolism can generate residues enriched in ^{13}C [9]. This interpretation is supported by the microbial community composition identified in CLT1, which is dominated by halotolerant and heterotrophic taxa such as *Salinisphaera* and hydrocarbon-degrading bacteria such as *Alcanivorax* [31]. These microorganisms are well suited to metabolize lipid- and hydrocarbon-rich substrates, including compounds derived from plant latex, and their preferential utilization of ^{1} ^{2}C during oxidative breakdown can result in ^{1} ^{3}C-enriched residual organic matter. Alternative or complementary contributions, such as carbonate-associated organic carbon or minor chemoautotrophic inputs, cannot be fully excluded. However, the dominance of microbial-derived markers in the Py-GC/MS spectra (e.g., alkyl nitriles, microbial lipids) strongly supports microbial activity as the primary driver.

The consistent ^{13}C-enrichment across compound families in CLT1 points to microbial reworking as a pervasive process, potentially through both degradation of surface-derived inputs and biosynthesis of new microbial metabolites. The enrichment of sterols such as A-Neo-oleana-3(5),12-diene and germanicol is particularly notable, as their values in CLT1 are much higher than in plant and soil counterparts (Table S3). This enrichment is consistent with microbial modification or biosynthesis of sterol-like structures [65,66], reinforcing their potential as microbial biomarkers within speleothem matrices.

At the same time, isotope heterogeneity across samples and compound classes may not be solely explained by microbial activity. Variability could reflect temporal heterogeneity in organic matter deposition, with compounds preserved from periods when environmental and hydrological conditions differed [67,68]. Surface disturbances such as wildfires, deforestation, or land-use change may also introduce isotope variability into cave deposits [5,23,35].

Intra-sample contrasts between compound classes further illustrate biosynthetic and metabolic fractionations (Fig. 4C). Polysaccharides and lignin typically show ^{13}C-enrichment, while lipids (fatty acids, alkanes, sterols) are ^{13}C-depleted due to isotope fractionation during lipid biosynthesis pathways [69–71]. The ^{13}C-enrichment of aromatic compounds in CLT1 may reflect microbial defunctionalization of lignin precursors such as methoxyphenols, a pathway known to retain heavier carbon isotopes [11–13,55].

Compound-specific carbon isotope analysis ($\delta^{13}C$) can help determine which of the hypotheses outlined in Section 4.1 best explains the origin of the organic matter in sample CLT1. The limited correspondence between several compound classes in CLT1 and their counterparts in the plant samples suggests that the most plausible scenarios are: (i) the presence of legacy organic matter derived from C_4 plants, and/or (ii) microbial alteration of latex exudates from *Euphorbia balsamifera*, which leached and percolated into the volcanic cave. The identification of *Alcanivorax* may support this hypothesis [31]. Although δ^{1} ^{3}C values in *Euphorbia* species vary with climate [33], Lanzarote's warm, arid setting, together with the isotope signatures across compound families (Fig. 4C), is consistent with a predominantly C_3 signal.

4.3.2. Hydrogen isotope composition

The similarity between $\delta^{2}H$ values in PCLT and SCLT can be explained by the absence of hydrogen isotope fractionation during root water uptake, as water absorbed by plants closely resembles the soil water isotope composition [72]. Since plant biomass is the main source of organic matter in the soil, the $\delta^{2}H$ values of soil reflect those of vegetation inputs [9,11]. The relatively uniform $\delta^{2}H$ across compound families in SCLT may therefore reflect the presence of different organic carbon pools of varying origin and/or age, which average out isotope differences [11].

In PCLT, intra-sample $\delta^{2}H$ variability is consistent with biosynthetic fractionations (Fig. 4C). Carbohydrate-derived polysaccharides displayed the highest $\delta^{2}H$ enrichment, which may be linked to hydrogen exchange during isomerization and polymerization reactions [73,74]. Lipids (*n*-alkanes/alkenes, fatty acids, sterols) were more depleted, reflecting isotope effects during biosynthesis [75] and incorporation of heavy hydrogen isotopes from NADPH [30,76]. Within lipids, sterols were the most depleted, consistent with previous findings distinguishing linear lipids and sterols [77]. Lignin compounds (methoxyphenols) showed $\delta^{2}H$ enrichment, which may be related to reduced stomatal conductance under environmental stress [78].

The marked ^{2}H-enrichment of CLT1 compounds, and especially of lignin-derived methoxyphenols, suggests incorporation of organic matter reflecting past hydrological conditions. Methoxyphenols are stable against microbial alteration [79], which supports the interpretation that their $\delta^{2}H$ values (–15.8‰ in CLT1) reflect the isotope composition of rainwater at the time of synthesis [80]. This interpretation is consistent with bulk $\delta^{2}H$ data (Table 1) and the recognition of speleothems as archives of paleoenvironmental change [5,23,35]. The strong enrichment relative to current vegetation further suggests that the organic fraction in CLT1 derives from older biomass inputs, incorporated via leaching into the speleothem, rather than from recent microbial alteration.

These results highlight that, although bulk hydrogen isotope analysis (Table 1) initially suggested microbial reworking as the main control, a high-resolution isotope analysis of individual chemical compounds by Py-CSIA reveals a stronger climatic and hydrological signal. The ability of Py-CSIA to discriminate between microbial processing and paleoenvironmental imprints underscores its precision and reliability for tracing organic matter sources and transformations [9,11].

4.4. Relevance of Py-CSIA for Mars biosignature exploration: opportunities, feasibility and limitations

The combined molecular and compound-specific isotope information obtained by Py-CSIA provides a powerful framework for evaluating the origin, preservation, and environmental context of organic matter in mineral matrices relevant to planetary exploration. By linking specific molecular structures with their δ^{1} ^{3}C and $\delta^{2}H$ signatures, Py-CSIA enables a more robust discrimination between biological, abiotic, and altered organic sources than molecular distributions alone, particularly in systems where organics occur at low concentrations and are strongly mineral-bound.

In this context, speleothems and mineral deposits formed within lava tubes represent especially valuable targets. These environments can act as protected archives of organic matter, shielding biosignatures from surface radiation, oxidative stress, and extreme temperature fluctuations [81,82]. The Lanzarote lava tube system, characterized by sparse vegetation, arid conditions, and volcanic substrates, is widely regarded as a Mars-analog environment, making it a relevant natural laboratory for testing biosignature detection strategies and assessing the preservation potential of organic compounds under conditions comparable to those expected on Mars [6,7,31,83].

Despite its strong potential to constrain biosignatures of past and present life and to reconstruct environmental conditions, carbon ($\delta^{13}C$) and hydrogen ($\delta^{2}H$) Py-CSIA is not currently feasible for in situ Mars operations using existing rover payloads. Implementation of this

approach requires a dedicated GC-combustion-IRMS system with precise control of carrier gases, oxidation reactors, calibration standards, and long-term instrumental stability. To date, such capabilities have not been deployed on Mars, where instruments such as SAM and MOMA provide GC-MS, pyrolysis, and/or laser desorption mass spectrometry, but not compound-specific isotope ratio measurements [4].

Analytical sensitivity further constrains potential in situ applications. Under terrestrial laboratory conditions, reliable $\delta^{1\ 3}C$ and δ^2H measurements by GC-IRMS typically require on-column loads on the order of ~1 nmol C (≈10 ng C) per compound to achieve robust precision. This implies that, without efficient preconcentration, target compounds would need to be present at approximately ppm levels in the analyzed sample. Such concentrations exceed many of the organic abundances reported to date on Mars, including chlorobenzene detected at ~150–300 ppbw in Gale crater mudstones [60]. These challenges are further compounded by the presence of oxychlorine phases, such as perchlorates, which can promote oxidation and chlorination reactions during pyrolysis, complicating the attribution of detected compounds to native precursors and potentially affecting isotopic integrity.

Accordingly, while Py-CSIA is currently best suited for Mars-analog studies on Earth and for the analysis of returned samples, its future in situ implementation would require next-generation isotope-ratio instrumentation coupled with robust preconcentration and cleanup strategies. If such technological advances are achieved, Py-CSIA would represent a major step forward in planetary organic geochemistry, enabling improved discrimination of organic sources and more quantitative reconstructions of past environmental conditions on Mars and other planetary bodies.

5. Conclusions

This study demonstrates the potential of Py-CSIA as a high-resolution tool to identify microbial biomarkers, as well as to investigate the origin and transformation of organic matter in Mars analogue lava tubes. By comparing two contrasting speleothem samples from the Corona Lava Tube (CLT1: black, jelly-like organic mat; and CLT3: white, cotton-like mineral deposits), we show that molecular- and isotope-level information provides insights that cannot be obtained from bulk analyses alone. Specifically, $\delta^{13}C$ and δ^2H signatures of individual compounds revealed evidence of: (i) intense microbial processing of plant-derived inputs, mainly from *Euphorbia balsamifera*, the dominant local vegetation, in CLT1, and (ii) incorporation of meteoric water and possible chemoautotrophic contributions in CLT3.

Beyond characterizing the biogeochemistry of Lanzarote's volcanic caves, our results highlight the value of analytical pyrolysis and specifically the Py-CSIA for life-detection strategies. The ability to distinguish between biogenic and abiogenic molecular signatures under conditions of low organic matter content makes this technique particularly relevant for planetary exploration. Applied to Martian lava tubes, Py-GC/MS and Py-CSIA could help identify diagnostic biomarkers and reconstruct past hydrological conditions, providing critical evidence for habitability and potential life beyond Earth.

CRediT authorship contribution statement

Nicasio T. Jiménez-Morillo: Writing – review & editing, Writing – original draft, Investigation, Formal analysis, Conceptualization. **Layla M. San-Emeterio:** Writing – review & editing, Writing – original draft, Investigation, Formal analysis. **José M. De la Rosa:** Writing – review & editing, Writing – original draft, Investigation, Formal analysis. **José A. González-Pérez:** Writing – review & editing, Resources, Investigation. **Francesco Sauro:** Writing – review & editing, Resources, Investigation. **Ana Z. Miller:** Writing – review & editing, Writing – original draft, Investigation, Funding acquisition, Conceptualization.

Declaration of Competing Interest

The authors declare that they have no known competing financial interests or personal relationships that could have appeared to influence the work reported in this paper.

Acknowledgements

This work was supported by the Spanish Ministry of Science and Innovation (MCIN/AEI/ 10.13039/501100011033) under the research project TUBOLAN PID2019–108672RJ-I00 and by the Spanish National Research Council (CSIC) through the intramural project PIE_20214AT021. This work was also supported by the HERMES project (ref. PID2024–162087NB-C21) funded by MICIU/AEI/10.13039/501100011033/. We acknowledge the financial support from the Portuguese Foundation for Science and Technology (FCT) under the MICROCENO project (10.54499/PTDC/CTA-AMB/0608/2020), and from the MICROLAVA project (PROYEXCEL_00185) funded by the Andalusia Regional Government. N.T.J.M. thanks the support from the Ramón y Cajal contract (RyC2021–031253-I) funded by MCIN/AEI/10.13039/501100011033 and the European Union "NextGenerationEU"/PRTR.

We thank the Cabildo de Lanzarote and the Lanzarote and Chinijo Archipelago Geopark for granting permission to access the La Corona Lava Tube system and collect samples. Field activities and sample collection were partially supported by the ESA PANGAEA-X training program. We are grateful to ESA astronaut Matthias Maurer for his dedicated involvement in collecting the samples analyzed in this study during the field training. We also thank Loredana Bessone, director of ESA's PANGAEA program, for her leadership and support in facilitating this multidisciplinary campaign.

Appendix A. Supporting information

Supplementary data associated with this article can be found in the online version at doi:10.1016/j.jaap.2026.107756.

Data availability

Data will be made available on request.

References

[1] I. Tomasi, M. Tonello, M. Massironi, P.A. Tesson, F. Sauro, C.M. Meyzen, et al., Geology of Lanzarote's northern region (Canary Island, Spain), J. Maps 19 (2023) 2187717, https://doi.org/10.1080/17445647.2023.2187717.

[2] F. Sauro, R. Pozzobon, M. Massironi, P. De Berardinis, T. Santagata, J. De Waele, Lava tubes on Earth, Moon and Mars: a review on their size and morphology revealed by comparative planetology, EarthSci. Rev. 209 (2020) 103288, https://doi.org/10.1016/j.earscirev.2020.103288.

[3] L. Carrer, R. Pozzobon, F. Sauro, et al., Radar evidence of an accessible cave conduit on the Moon below the Mare Tranquillitatis pit, Nat. Astron. 8 (2024) 1119–1126, https://doi.org/10.1038/s41550-024-02302-y.

[4] F. Goesmann, W.B. Brinckerhoff, F. Raulin, et al., The Mars Organic Molecule Analyzer (MOMA) instrument: characterization of organic material in martian sediments, Astrobiology 17 (2017) 655–685, https://doi.org/10.1089/ast.2016.1551.

[5] A.Z. Miller, J.M. De la Rosa, N.T. Jiménez-Morillo, M.F.C. Pereira, J.A. González-Pérez, J.M. Calaforra, C. Saiz-Jimenez, Analytical pyrolysis and light stable isotope analyses reveal environmental changes in coralloid speleothems from Easter Island, J. Chromatogr. A 1461 (2016) 144–152, https://doi.org/10.1016/j.chroma.2016.07.038.

[6] V. Palma, J.M. De la Rosa, B.P. Onac, et al., Decoding organic compounds in lava tube sulfates to understand potential biomarkers in the Martian subsurface, Commun. Earth Environ. 5 (2024) 530, https://doi.org/10.1038/s43247-024-01673-4.

[7] V. Palma, J.L. González-Pimentel, N.T. Jiménez-Morillo, F. Sauro, et al., Connecting molecular biomarkers, mineralogical composition, and microbial diversity from Mars analog lava tubes, Sci. Total Environ. 913 (2024) 169583, https://doi.org/10.1016/j.scitotenv.2023.169583.

[8] J. Hayes, Fractionation of carbon and hydrogen isotopes in biosynthetic processes, Rev. Mineral. Geochem. 43 (2001) 225–277, https://doi.org/10.2138/gsrmg.43.1.225.

[9] N.T. Jiménez-Morillo, G. Almendros, F.J. González-Vila, A. Jordán, L.M. Zavala, J. M. De la Rosa, J.A. González-Pérez, Fire effects on C and H isotopic composition in plant biomass and soil: bulk and particle size fractions, Sci. Total Environ. 749 (2020) 141417, https://doi.org/10.1016/j.scitotenv.2020.141417.

[10] M.J. Selensky, A.L. Masterson, J.G. Blank, S.C. Lee, M.R. Osburn, Stable carbon isotope depletions in lipid biomarkers suggest subsurface carbon fixation in lava caves, J. Geophys. Res. Biogeosci. 126 (2021) e2021JG006430, https://doi.org/10.1029/2021JG006430.

[11] L.M. San-Emeterio, L.M. Zavala, N.T. Jiménez-Morillo, I.M. Pérez-Ramos, J. A. González-Pérez, Effects of climate change on soil organic matter C and H isotope composition in a Mediterranean Savannah (Dehesa): an assessment using Py-CSIA, Environ. Sci. Technol. 57 (2023) 13851–13862, https://doi.org/10.1021/acs.est.3c01816.

[12] L.M. San-Emeterio, N.T. Jiménez-Morillo, I.M. Pérez-Ramos, M.-T. Domínguez, J. A. González-Pérez, Changes in soil organic matter molecular structure after five-years mimicking climate change scenarios in a Mediterranean savannah, Sci. Total Environ. 857 (2023) 159288, https://doi.org/10.1016/j.scitotenv.2022.159288.

[13] L.M. San-Emeterio, N.T. Jiménez-Morillo, L. Reina, V. Vinciguerra, P. Menendez, J. A. González-Pérez, Pyrolysis carbon compound-specific isotope analysis (Py-CSIA) of *Eucalyptus* spp. bark and the extracted lignin, J. Anal. Appl. Pyrolysis 170 (2023) 105896, https://doi.org/10.1016/j.jaap.2023.105896.

[14] J.S. Fang, C. Li, L. Zhang, T. Davis, C. Kato, D.H. Bartlett, Hydrogen isotope fractionation in lipid biosynthesis by the piezophilic bacterium Moritella japonica DSK1, Chem. Geol. 367 (2014) 34–38, https://doi.org/10.1016/j.chemgeo.2013.12.018.

[15] W.D. Leavitt, T.M. Flynn, M.K. Suess, A.S. Bradley, Transhydrogenase and growth substrate influence lipid hydrogen isotope ratios in Desulfovibrio alaskensis G20, Front. Microbiol. 7 (2016) 918, https://doi.org/10.3389/fmicb.2016.00918.

[16] D. Sachse, I. Billault, G.J. Bowen, Y. Chikaraishi, T.E. Dawson, S.J. Feakins, K. H. Freeman, et al., Molecular Paleohydrology: interpreting the hydrogen-isotopic composition of lipid biomarkers from photosynthesizing organisms, Annu. Rev. Earth Planet. Sci. 40 (2012) 221–249, https://doi.org/10.1146/annurev-earth-042711-105535.

[17] R.S. Wijker, A.L. Sessions, T. Fuhrer, M. Phan, $^{2}H/^{1}H$ variation in microbial lipids is controlled by NADPH metabolism, Proc. Natl. Acad. Sci. U.S.A. 116 (2019) 12173–12182, https://doi.org/10.1073/pnas.1818372116.

[18] Y.A. Taran, G.A. Kliger, E. Cienfuegos, A.N. Shuykin, Carbon and hydrogen isotopic compositions of products of open-system catalytic hydrogenation of CO_2: Implications for abiogenic hydrocarbons in Earth's crust, Geochim. Cosmochim. Acta 74 (2010) 6112–6125, https://doi.org/10.1016/j.gca.2010.08.012.

[19] E.P. Reeves, J.S. Seewald, S.P. Sylva, Hydrogen isotope exchange between n-alkanes and water under hydrothermal conditions: Implications for abiotic and thermogenic hydrocarbons in vent fluids, Geochim. Cosmochim. Acta 77 (2012) 582–599, https://doi.org/10.1016/j.gca.2011.10.008.

[20] F. Sauro, S.J. Payler, M. Massironi, R. Pozzobon, H. Hiesinger, N. Mangold, C. S. Cockell, J. Martínez Frias, K. Kullerud, L. Turchi, I. Drozdovskiy, L. Bessone, Training astronauts for scientific exploration on planetary surfaces: The ESA PANGAEA programme, Acta Astronaut 204 (2023) 222–238, https://doi.org/10.1016/j.actaastro.2022.12.034.

[21] N.T. Jiménez-Morillo, V. Palma, R. Garcia, C.B. Dias, M.J. Cabrita, Combination of stable isotope analysis and chemometrics to discriminate geoclimatically and temporally the virgin olive oils from three mediterranean countries, Foods 9 (2020) 1855, https://doi.org/10.3390/foods9121855.

[22] L.M. San-Emeterio, N.T. Jiménez-Morillo, J.A. Vega, C. Fernández, T. Fonturbel, G. Almendros, J.A. González-Pérez, Effects of fire severity on soil organic matter: a multi-isotope (C, N, H, O) comparison of wildfires and experimental burns, Catena 264 (2026) 109817, https://doi.org/10.1016/j.catena.2026.109817.

[23] A.Z. Miller, N.T. Jiménez-Morillo, M.L. Coutinho, F. Gazquez, V. Palma, et al., Organic geochemistry and mineralogy suggest anthropogenic impact in speleothem chemistry from volcanic show caves of the Galapagos, iScience 25 (2022) 104556, https://doi.org/10.1016/j.isci.2022.104556.

[24] I.D. Bull, P.F. Bergen, C.J. Nott, P.R. Poulton, R.P. Evershed, Organic geochemical studies of soils from the Rothamsted classical experiments—V. The fate of lipids in different long-term experiments, Org. Geochem. 31 (2000) 389–408, https://doi.org/10.1016/S0146-6380(00)00008-5.

[25] N.T. Jiménez-Morillo, J.M. De la Rosa, D. Waggoner, G. Almendros, F.J. González-Vila, J.A. González-Pérez, Fire effects in the molecular structure of soil organic matter fractions under *Quercus suber* cover, Catena 145 (2016) 266–273, https://doi.org/10.1016/j.catena.2016.06.022.

[26] P. Leinweber, H.-R. Schulten, Composition, stability and turnover of soil organic matter: Investigations by off-line pyrolysis and direct pyrolysis-mass spectrometry, J. Anal, Appl, Pyrolysis 32 (1995) 91–110.

[27] F.J González-Vila, P. Tinoco, G. Almendros, F. Martin, Py-CG-MS analysis of the formation and degradation stages of charred residues from lignocellulosic biomass, J. Agric. Food Chem. 49 (3) (2001) 1128–1131, https://doi.org/10.1021/jf0006325.

[28] M.E. Arias, O. Polvillo, J. Rodríguez, M. Hernandez, J.A. Gonzalez-Perez, F. J. Gonzalez-Vila, Thermal transformations of pine wood components under pyrolysis/gas chromatography/mass spectrometry conditions, J. Anal. Appl. Pyrolysis 77 (2005) 63–67, https://doi.org/10.1016/j.jaap.2005.12.013.

[29] G. Almendros, P. Tinoco, J.M. De la Rosa, H. Knicker, J.A. González-Pérez, F. J. González-Vila, Selective effects of forest fires on the structural domains of soil humic acids as shown by dipolar dephasing ^{13}C NMR and graphical-statistical analysis of pyrolysis compounds, J. Soil Sediment 18 (2018) 1303–1313, https://doi.org/10.1007/s11368-016-1595-y.

[30] N.T. Jiménez-Morillo, M.J. Cabrita, C.B. Dias, F.J. González-Vila, J.A. González-Pérez, Pyrolysis-compound-specific hydrogen isotope analysis ($\delta^{2}H$ Py-CSIA) of Mediterranean olive oils, Food Control 110 (2020) 107023, https://doi.org/10.1016/Fj.foodcont.2019.1070.

[31] A.Z. Miller, J.L. González-Pimentel, J.M. De la Rosa, S. Gutiérrez-Patricio, N. T. Jiménez-Morillo, et al., The Microbial Inhabitants of the Corona Lava Tube: astrobiological Insights from a Mars Analog Environment, Astrobiology 26 (2026) 30–47, https://doi.org/10.1177/15311074251413229.

[32] B. Fry, Stable Isotope Ecology, Springer, New York, 2006.

[33] R.W. Pearcy, J. Troughton, C4 photosynthesis in tree form euphorbia species from hawaiian rainforest sites, Plant Physiol. 55 (1975) 1054–1056, https://doi.org/10.1104/pp.55.6.1054.

[34] Y. Yanes, C.S. Romanek, A. Delgado, H.A. Brant, J.E. Noakes, M.R. Alonso, M. Ibáñez, Oxygen and carbon stable isotopes of modern land snail shells as environmental indicators from a low-latitude oceanic island, Geochim. Cosmochim. Acta 73 (2009) 4077–4099, https://doi.org/10.1016/j.gca.2009.04.021.

[35] A.Z. Miller, J.M. De la Rosa, N.T. Jiménez-Morillo, M.F.C. Pereira, J.A. González-Pérez, H. Knicker, C. Saiz-Jimenez, Impact of wildfires on subsurface volcanic environments: new insights into speleothem chemistry, Sci. Total Environ. 698 (2020) 134321, https://doi.org/10.1016/j.scitotenv.2019.134321.

[36] J. Cosford, H. Qing, D. Mattey, B. Eglington, M. Zhang, Climatic and local effects on stalagmite $\delta^{13}C$ values at Lianhua Cave, China, Palaeogeogr. Palaeoclimatol. Palaeoecol. 280 (2009) 235–244, https://doi.org/10.1016/j.palaeo.2009.05.020.

[37] T.E. Dawson, S. Mambelli, A.H. Plamboeck, et al., Stable isotopes in plant ecology, Annu. Rev. Ecol. Syst. 33 (2002) 507–559, https://doi.org/10.1146/annurev.ecolsys.33.020602.095451.

[38] A. Girona-García, D. Badía-Villas, N.T. Jiménez-Morillo, J.M. De la Rosa, J. A. González-Pérez, Soil C and N isotope composition after a centennial Scots pine afforestation in podzols of native European beech forests in NE-Spain, Catena 165 (2018) 434–441, https://doi.org/10.1016/j.catena.2018.02.023.

[39] P. Szpak, Complexities of nitrogen isotope biogeochemistry in plant–soil systems: implications for the study of ancient agricultural and animal management practices, Front. Plant Sci. 5 (2014) 1–19, https://doi.org/10.3389/fpls.2014.00288.

[40] S. Wankel, C. Buchwald, W. Ziebis, C. Wenk, M. Lehmann, Nitrogen cycling in the deep sedimentary biosphere: nitrate isotopes in porewaters underlying the oligotrophic North Atlantic, Biogeosciences 12 (2015) 7483–7502, https://doi.org/10.5194/BG-12-7483-2015.

[41] P.Z. Ellsworth, D.G. Williams, Hydrogen isotope fractionation during water uptake by woody xerophytes, Plant Soil 291 (2007) 93–107.

[42] F. Cui, J. Liu-Zeng, Y. Li, Q. Xu, M. Tang, H. Wang, Z. Sun, Principle of Hydrogen Isotope Geochemistry Paleo-altimeter and its Potential in Reconstructing Paleo-elevation of the Southeastern Tibetan Plateau, Acta Geol. Sin. Engl. 98 (2024) 1051–1063, https://doi.org/10.1111/1755-6724.15196.

[43] P. Négrel, E. Petelet-Giraud, Isotopes in groundwater as indicators of climate changes, TRACTrend Anal. Chem. 30 (2011) 1279–1290, https://doi.org/10.1016/j, trac.2011.06.001.

[44] IAEA, WMO, Global Network of Isotopes in Precipitation (GNIP). International Atomic Energy Agency, Vienna, Austria 2010.

[45] S. Affolter, T. Kipfer, E. Hofmeister, M. Leuenberger, D. Fleitmann, Paleoclimatic significance of water isotopes in speleothem fluid inclusions, EarthSci. Rev. 261 (2024) 105026, https://doi.org/10.1016/j.earscirev.2024.105026.

[46] A. Fernandez, M.H. Løland, J. Maccali, Y. Krüger, H.B. Vonhof, H. Sodemann, A. N. Meckler, Characterization and correction of evaporative artifacts in speleothem fluid inclusion isotope analyses as applied to a stalagmite from Borneo, Geochem. Geophys. Geosyst 24 (2023) e2023GC010857, https://doi.org/10.1029/2023GC010857.

[47] R.S. Harmon, H.P. Schwarcz, J.R. O'Neil, D/H ratios in speleothem fluid inclusions: A guide to variations in the isotopic composition of meteoric precipitation? Earth Planet. Sci. Lett. 42 (1979) 254–266, https://doi.org/10.1016/0012-821X(79)90033-5.

[48] F. Held, H. Cheng, R.L. Edwards, T. Kipfer, O. Tüysüz, K. Koç, S. Affolter, D. Fleitmann, Hydrological variability in the Black Sea region during the last 670,000 years recorded in multi-proxy speleothem records from northern Türkiye, Quat. Sci. Rev. 367 (2025) 109534, https://doi.org/10.1016/j.quascirev.2025.109534.

[49] S. McGarry, M. Bar-Matthews, A. Matthews, A. Vaks, B. Schilman, A. Ayalon, Constraints on hydrological and paleotemperature variations in the Eastern Mediterranean region in the last 140 ka given by the δD values of speleothem fluid inclusions, Quat. Sci. Rev. 23 (2004) 919–934, https://doi.org/10.1016/j.quascirev.2003.06.020.

[50] E. Cassel, D. Breecker, Long-term stability of hydrogen isotope ratios in hydrated volcanic glass, Geochim. Cosmochim. Acta 200 (2017) 67–86, https://doi.org/10.1016/J.GCA.2016.12.001.

[51] M.E. Arias, A. Blánquez, M. Hernández, J. Rodríguez, A.S. Ball, N.T. Jiménez-Morillo, F.J. González-Vila, J.A. González-Pérez, Role of a thermostable laccase produced by *Streptomyces ipomoeae* in the degradation of wheat straw lignin in solid state fermentation, J. Anal. Appl. Pyrolysis 122 (2016) 202–208, https://doi.org/10.1016/j.jaap.2016.09.023.

[52] M. Afrokh, S. Tahrouch, K. ELMehrach, F. Fahmi, Ait Bihi, M. Weber-Ravn, H. Hatimi, A. Tabyaoui, M. Ethnobotanical, phytochemical and antioxidant study of fifty aromatic and medicinal plants, Chem. Data Collect 43 (2023) 100984, https://doi.org/10.1016/j.cdc.2022.100984.

[53] A. Rogowska, A. Szakiel, The role of sterols in plant response to abiotic stress, Phytochem. Rev. 19 (2020) 1525–1538, https://doi.org/10.1007/s11101-020-09708-2.
[54] N.T. Jiménez-Morillo, J.E. Spangenberg, A.Z. Miller, A. Jordán, L.M. Zavala, F. J. González-Vila, J.A. González-Pérez, Wildfire effects on lipid composition and hydrophobicity of bulk soil and soil size fractions under *Quercus suber* cover (SW-Spain), Environ. Res. 159 (2017) 394–405, https://doi.org/10.1016/j.envres.2017.08.022.
[55] E.S. Krull, J.O. Skjemstad, D. Graetz, K. Grice, W. Dunning, G. Cook, J.F. Parr, ^{13}C-depleted charcoal from C4 grasses and the role of occluded carbon in phytoliths, Org. Geochem. 34 (2003) 1337–1352, https://doi.org/10.1016/S0146-6380(03)00100-1.
[56] S. Labana, M. Kapur, D.K. Malik, D. Prakash, R. Jain, Diversity, Biodegradation and Bioremediation of Polycyclic Aromatic Hydrocarbons, in: S.N. Singh, R.D. Tripathi (Eds.), Environmental Bioremediation Technologies, Springer, Berlin, Heidelberg, 2007, pp. 409–443, https://doi.org/10.1007/978-3-540-34793-4_18.
[57] W. Wilcke, W. Amelung, M. Krauss, C. Martius, A. Bandeira, M. Garcia, Polycyclic aromatic hydro carbon (PAH) patterns in climatically different eco logical zones of Brazil, Org. Geochem. 34 (2003) 1405–1417, https://doi.org/10.1016/S0146-6380(03)00137-2.
[58] C. Saiz-Jimenez, J.W. De Leeuw, Lignin pyrolysis products: Their structures and their significance as biomarkers, Org. Geochem. 10 (1986) 869–876.
[59] G. Chiavari, G.C. Galletti, Pyrolysis–gas chromatography/mass spectrometry of amino acids, J. Anal. Appl. Pyrolysis 24 (1992) 123–137.
[60] C. Freissinet, D.P. Glavin, P.R. Mahaffy, K.E. Miller, J.L. Eigenbrode, R. E. Summons, et al., Organic molecules in the Sheepbed Mudstone, Gale Crater, Mars, J. Geophys. Res. Planets 120 (2015) 495–514, https://doi.org/10.1002/2014JE004737.
[61] C. Freissinet, D.P. Glavin, P.D. Archer, S. Teinturier, A. Buch, C. Szopa, et al., Long-chain alkanes preserved in a Martian mudstone, Proc. Natl. Acad. Sci. U. S. A. 122 (2025) e2420580122, https://doi.org/10.1073/pnas.2420580122.
[62] S. Sharma, R.D. Roppel, A.E. Murphy, et al., Diverse organic-mineral associations in Jezero crater, Mars, Nature 619 (2023) 724–732, https://doi.org/10.1038/s41586-023-06143-z.
[63] M.A. Goni, T.I. Eglinton, Stable carbon isotopic analyses of lignin-derived CuO oxidation products by isotope ratio monitoring gas chromatography mass spectrometry (irm-GC-MS), Org. Geochem. 24 (1996) 601–615.
[64] E.A. Hobbie, R.A. Werner, Intramolecular, compound-specific, and bulk carbon isotope patterns in C3 and C4 plants: a review and synthesis, N. Phytol. 161 (2004) 371–385, https://doi.org/10.1111/j.1469-8137.2004.00970.x.
[65] J. Jacob, J.-R. Disnar, G. Bardoux, Carbon isotope evidence for sedimentary miliacin as a tracer of *Panicum miliaceum* (broomcorn millet) in the sediments of Lake le Bourget (French Alps), Org. Geochem. 39 (2008) 1077–1080, https://doi.org/10.1016/j.orggeochem.2008.04.003.
[66] I. Kristen, H. Wilkes, A. Vieth, et al., Biomarker and stable carbon isotope analyses of sedimentary organic matter from Lake Tswaing: evidence for deglacial wetness and early Holocene drought from South Africa, J. Paleolimnol. 44 (2010) 143–160, https://doi.org/10.1007/s10933-009-9393-9.
[67] C.J. de Cisneros, E. Caballero, Carbon isotope values as paleoclimatic indicators. Study on stalagmite from Nerja Cave, South Spain, Carbonates Evaporites 26 (2011) 41–46, https://doi.org/10.1007/s13146-011-0049-2.
[68] F.A. Lechleitner, C.C. Day, O. Kost, M. Wilhelm, N. Haghipour, G.M. Henderson, H. M. Stoll, Stalagmite carbon isotopes suggest deglacial increase in soil respiration in western Europe driven by temperature change, Clim 17 (2021) 1903–1918, https://doi.org/10.5194/cp-17-1903-2021.
[69] A. Gilbert, R.J. Robins, G.S. Remaud, G.G. Tcherkez, Intramolecular ^{13}C pattern in hexoses from autotrophic and heterotrophic C3 plant tissues, Proc. Natl. Acad. Sci. U. S. A. 109 (2012) 18204–18209, https://doi.org/10.1073/pnas.1211149109.
[70] G. Tcherkez, A. Mahé, M. Hodges, ^{12}C/^{13}C fractionations in plant primary metabolism, Trends Plant Sci. 16 (2011) 499–506, https://doi.org/10.1016/j.tplants.2011.05.010.
[71] W. Zhao, J. Fang, X. Huang, Y. Zhang, W. Liu, Y. Wang, L. Zhang, Carbon and hydrogen isotope fractionation in lipid biosynthesis by *Sporosarcina* sp. DSK25, Geochem. Persp. Let. 14 (2020) 9–13, https://doi.org/10.7185/geochemlet.2016.
[72] J.R. Brook, H.R. Barnad, R. Coulombe, J.J. McDonnell, Ecohydrologic separation of water between trees and streams in a Mediterranean climate, Nat. Geosci. 3 (2010) 100–104, https://doi.org/10.1038/ngeo722.
[73] M.F. Estep, T.C. Hoering, Biogeochemistry of the stable hydrogen isotopes, Geochim. Cosmochim. Acta 44 (1980) 1197–1206, https://doi.org/10.1016/0016-7037(80)90073-3.
[74] A. Schimmelmann, A.L. Sessions, M. Mastalerz, Hydrogen isotopic (D/H) composition of organic matter during diagenesis and thermal maturation, Annu. Rev. Earth Planet Sci. 34 (2006) 501–533, https://doi.org/10.1146/annurev.earth.34.031405.125011.
[75] G.J. Martin, B.L. Zhang, N. Naulet, M.L. Martin, Deuterium transfer in the bioconversion of glucose to ethanol studied by specific isotope labeling at the natural abundance level, J. Am. Chem. Soc. 108 (1986) 5116–5122, https://doi.org/10.1021/ja00277a013.
[76] Y.-H. Luo, Ld.S.L. Sternberg, S. Suda, S. Kumazawa, A. Mitsui, Extremely low D/H ratios of photoproduced hydrogen by cyanobacteria, Plant Cell Physiol. 32 (1991) 897–900, https://doi.org/10.1093/oxfordjournals.pcp.a078158.
[77] A.L. Sessions, T.W. Burgoyne, A. Schimmelmann, J.M. Hayes, Fractionation of hydrogen isotopes in lipid biosynthesis, Org. Geochem. 30 (1999) 1193–1200, https://doi.org/10.1016/S0146-6380(99)00094-7.
[78] J. Rodríguez-Calcerrada, V. Chano, L. Matías, M.D. Hidalgo-Galvez, J. Cambrollé, I. M. Pérez-Ramos, Three years of warming and rainfall reduction alter leaf physiology but not relative abundance of an annual species in a Mediterranean savanna, J. Plant Physiol. 275 (2022) 153761, https://doi.org/10.1016/j.jplph.2022.153761.
[79] N.T. Jiménez-Morillo, J.A. González-Pérez, G. Almendros, J.M. De la Rosa, D. C. Waggoner, A. Jordán, L.M. Zavala, F.J. González-Vila, P.G. Hatcher, Ultra-high resolution mass spectrometry of physical speciation patterns of organic matter in fire-affected soils, J. Environ. Manag. 25 (2018) 139–147, https://doi.org/10.1016/j.jenvman.2018.07.069.
[80] F. Keppler, D.B. Harper, R.M. Kalin, W. Meier-Augenstein, N. Farmer, et al., Blackwell Publishing Ltd Stable hydrogen isotope ratios of lignin methoxyl groups as a paleoclimate proxy and constraint of the geographical origin of Wood, N. Phytol. 176 (2007) 600–609, https://doi.org/10.1111/j.1469-8137.2007.02213.x.
[81] N. Hadland, C.W. Hamilton, S. Duhamel, Young volcanic terrains are windows into early microbial colonization, Commun. Earth Environ. 5 (2024) 114, https://doi.org/10.1038/s43247-024-01280-3.
[82] B.L. Carrier, D.W. Beaty, M.A. Meyer, et al., Mars Extant Life: What's Next? Conference Report, Astrobiology 20 (2020) 785–814, https://doi.org/10.1089/ast.2020.2237.
[83] V. Palma, J.M. De la Rosa, F. Sauro, B.P. Onac, M. Massironi, S. Gutierrez-Patricio, A.T. Caldeira, F. Gázquez, N.T. Jiménez-Morillo, A.Z. Miller, Exploring organic biomarkers in lava tube gypsum deposits using analytical pyrolysis, J. Anal. Appl. Pyrolysis 192 (2025) 107245, https://doi.org/10.1016/j.jaap.2025.107245.